



DØnote 4510-CONF

Search for Single Top Quark Production at DØ in Run II

The DØ Collaboration
URL <http://www-d0.fnal.gov>
(Dated: August 13, 2004)

Version 1.31

We present a search for single top quark production. The search is performed in the electron+jets and muon+jets decay channels with a b -quark tagged jet. We use between 156 pb^{-1} and 169 pb^{-1} of Run II data, depending on the analysis channel, collected between August 2002 and September 2003. The resulting 95% confidence level upper limits on the production cross sections are 19 pb (s -channel production), 25 pb (t -channel production), and 23 pb ($s+t$ channel production).

Preliminary Results for Summer 2004 Conferences

I. INTRODUCTION

The top quark, discovered by the Tevatron CDF and DØ collaborations [1, 2] is the heaviest elementary particle found so far. The top quark mass measurement by CDF and DØ in Run I gives $m_t = 178.0 \pm 4.3$ GeV [3], which is in good agreement with the result from the electroweak data analysis by LEP and SLC [4], 179_{-9}^{+11} GeV. Despite the fact that the top quark is so heavy, it is predicted to be a point-like particle in the Standard Model (SM). The top quark is much heavier than all other quarks and its mass is not far from the electroweak scale, and the top Yukawa coupling $\lambda_t = 2^{3/4} G_F^{1/2} m_t$ is very close to unity. Because of these and other unusual top quark properties, one expects that a study of top quark physics might reveal details of the electroweak symmetry breaking mechanism or new physics [5, 6].

Top quarks, pair produced via the strong force, have been observed at the Tevatron. However, the SM predicts that top quarks should also be produced singly through electroweak interactions. Single top production mechanisms and related top quark physics have been the subject of many studies, see for example [7]: a measurement of the single top cross section can be used to obtain a limit on the magnitude of the CKM matrix element V_{tb} , to measure the top quark width Γ_t , and to study the properties of the Wtb coupling.

In Fig. 1 we show the most important Feynman diagrams for single top production at the Tevatron.



FIG. 1: The dominant Feynman diagrams for s -channel (left) and t -channel (right) single top quark production.

These two processes, referred to as the s -channel and t -channel processes, may be characterized by the virtuality Q_W^2 , that is, the four-momentum squared, of the participating W -boson:

- t -channel W -exchange ($Q_W^2 < 0$): This process, $p\bar{p} \rightarrow tq\bar{b} + X$, has the largest cross section of the single top processes. We refer to the t -channel process as “ tqb ,” which includes $tq\bar{b}$, $\bar{t}q\bar{b}$, tq , and $\bar{t}\bar{q}$. The next-to-leading order (NLO) cross section is $1.98_{-0.18}^{+0.23}$ pb [8, 9] at $\sqrt{s} = 1.96$ TeV with $m_t = 175$ GeV.
- s -channel W -exchange ($Q_W^2 > 0$): The NLO cross section for this process, $p\bar{p} \rightarrow t\bar{b} + X$, is $0.88_{-0.06}^{+0.07}$ pb [10] at $\sqrt{s} = 1.96$ TeV with $m_t = 175$ GeV. We refer to the s -channel process as “ tb ,” which includes both $t\bar{b}$ and $\bar{t}b$.

Searches for single top production were carried out in Run I, but the integrated luminosity of about 90 pb^{-1} was not enough for an observation. Upper limits on the cross sections were published by both the DØ [11, 12] and CDF [13, 14] collaborations. At the 95% confidence level, DØ’s upper limit on the s -channel production cross section is 17 pb and the CDF limit is 18 pb. At the same confidence level, the upper limit on the t -channel is 22 pb by DØ and 13 pb by CDF. CDF also published a combined limit of 14 pb.

In Run II at the Tevatron, a discovery of electroweak top quark production is expected owing to the significantly higher luminosity and much better b -quark identification. We report here on the first search for single top production in the Run II data with the upgraded DØ detector [15]. The search uses $p\bar{p}$ data at $\sqrt{s} = 1.96$ TeV collected between August 2002 and September 2003. The integrated luminosity used in the analysis varies from 156 to 169 pb^{-1} depending upon the particular signal channel. No signal is observed, and limits are set on the production cross section.

II. DATA AND MONTE CARLO

The analysis is partitioned by decay channel and b -quark identification method. The integrated luminosity used for the analysis of the electron channel with the soft lepton b -tag is 156 pb^{-1} . For electrons with the lifetime b -tag, 169 pb^{-1} is used, and for muons 158 pb^{-1} is used for both b -tagging methods. The different luminosities are due to data quality requirements.

The initial electron dataset is made up of events containing a reconstructed electromagnetic object with transverse energy $E_T > 12$ GeV deposited in the calorimeter, and a track with transverse momentum $p_T > 8$ GeV. The initial muon dataset is made up of events containing a track matched with a muon stub in the outer spectrometer. We also use a multijet sample to measure the probability that a jet originated from a B hadron. This sample contains events that have satisfied a simple multijet online trigger requirement.

The single top signals are modeled with a custom implementation of CompHEP [16] known as SingleTop [17], which reproduces the next-to-leading order kinematic distributions of the decay particles in s -channel and t -channel production, including the decay angles. These parton-level events are processed with PYTHIA [18] to add the underlying event from the proton-antiproton interaction, to include initial-state and final-state radiation, and to hadronize the quarks and gluons into jets. Tau leptons are decayed using TAUOLA [19] and B hadrons are decayed using EVTGEN [21]. The $t\bar{t}$ background is modeled at leading order using ALPGEN [22], with PYTHIA, TAUOLA, and EVTGEN as described for the single top samples. The $t\bar{t}$ cross section is scaled to the NLO cross section calculation [20]. The top quark mass for these samples is 175 GeV. For the s -channel and $t\bar{t}$ samples, $Q^2 = m_t^2$. For the t -channel samples, $Q^2 = (m_t/2)^2$. The parton distribution functions used are CTEQ6M [23] for the single top event samples and CTEQ6.1M for the $t\bar{t}$ samples. The $Z \rightarrow \mu\mu$ +jets background is modeled with ALPGEN.

The Monte Carlo event samples are processed with a full GEANT [24]-based simulation of the DØ detector, and the resulting lepton and jet energies are smeared to reproduce the resolutions observed in data.

Figure 2 shows the transverse momenta and pseudorapidities for the partons in our Monte Carlo models of the s -channel and t -channel single top processes, after decay of the top quark and W boson. The most unusual feature is the forward direction of the light quark in t -channel production, shown in green in the lower right-hand plot. The \bar{b} quark in this channel (shown in black) has very low momentum and a broad η distribution, so is not often reconstructed or tagged.

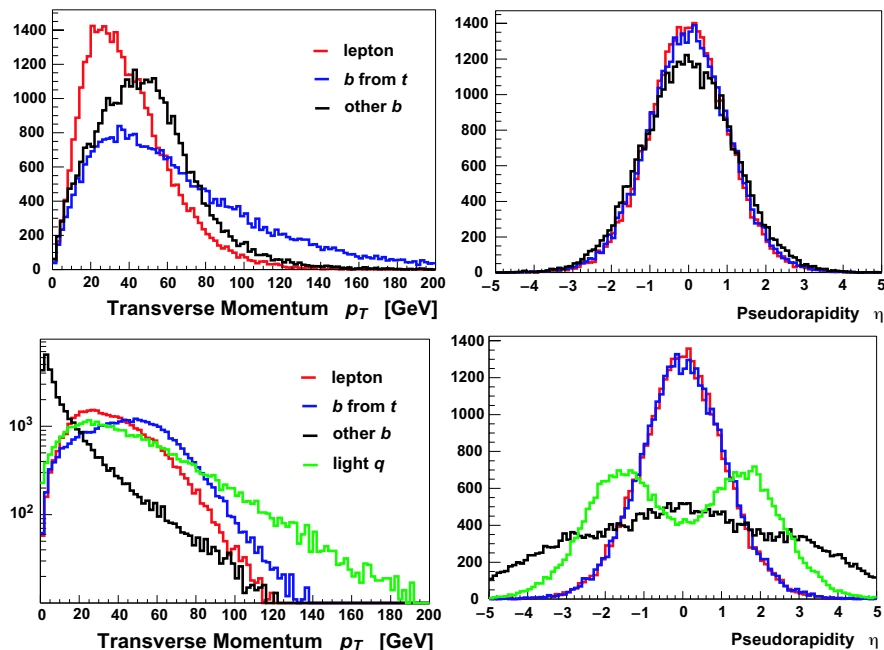


FIG. 2: Distributions of transverse momenta (left column) and pseudorapidity (right column) for the final-state partons in s -channel single top events (upper row) and t -channel (lower row). The plots show t and \bar{t} combined.

III. EVENT TOPOLOGY

The final state signature of a single top quark event is characterized by the decay of the top quark ($t \rightarrow Wb$): one centrally produced high- p_T lepton, large missing transverse energy from the neutrino (\cancel{E}_T), one high- p_T central b quark jet from the top decay, one associated b quark jet, and one light quark (t -channel). Processes with similar final states include W +jets events, $t\bar{t}$, $b\bar{b}$, multijet events with a jet misidentified as an electron, and some smaller contributions from Z +jets and diboson events, as further described below:

- W +jets production. This is the dominant background. $Wb\bar{b}$ is an irreducible background for the s-channel and $Wb\bar{b}g$ is irreducible for the t-channel.
- $t\bar{t}$ production. This process has a larger multiplicity of final particles than single top events. However, if jets or a lepton are not properly reconstructed or lost in detector cracks, the kinematics of the remaining particles are very similar to those of the single top signal.
- Multijet events. This background can manifest itself by a jet faking an electron or a muon in a b -quark decay faking an isolated muon. The probability of a jet faking an electron is rather small, about 10^{-4} , but the ≥ 3 jet cross section is large, resulting in a small but non-negligible contribution to the background. $b\bar{b}$ production contributes to the background when one of the b 's decays semileptonically and the electron or muon is mistaken for one from a W boson decay. This is mainly a background in the $W \rightarrow \mu\nu$ channel.
- $Z/\text{Drell-Yan}$ +jets production can mimic the single top signals in two ways. There are two isolated leptons (e^+e^- or $\mu^+\mu^-$) in the final state, but if one lepton is not reconstructed, then this results in missing transverse energy, which can reconstruct as a W boson when combined with the other lepton. Further $Z/\text{Drell-Yan}$ +jets in the $\mu^+\mu^-$ final state can contribute if a muon overlaps with a jet, thereby identified as a tagging muon from a semileptonic b decay.
- WW , WZ , and ZZ processes are the electroweak part of the W +jets and Z +jets backgrounds. The cross sections are a few picobarns each.

IV. EVENT RECONSTRUCTION

Electrons are reconstructed using information from both the calorimeter and the central tracker. The electromagnetic (EM) calorimeter cluster must have $E_T > 15$ GeV and be within the central calorimeter module (detector pseudorapidity $|\eta^{\text{det}}| < 1.1$). Additional requirements on the cluster include a matched central track and a threshold requirement on a seven-variable likelihood that includes many of the cluster and track properties.

Muons are reconstructed using information from the muon spectrometer (detector pseudorapidity $|\eta^{\text{det}}| < 2$). Additional requirements include requiring a good match to a central track, requiring the muon be outside any jet's cone ($\Delta R(\mu, \text{jet}) > 0.5$), and requiring isolation from activity in both the tracker and the calorimeter. Muons used in the soft lepton tagging of b -jets are not required to have a match with a central track, but are required to have $E_T > 4$ GeV and to be within $\Delta R \leq 0.5$ of the jet axis. Timing from scintillator hits is used for cosmic-ray rejection.

Jets are reconstructed using a mid-point cone algorithm with radius $R = 0.5$. Jets are required to have $E_T > 15$ GeV and $|\eta^{\text{det}}| \leq 3.4$. Each event is required to have between two and four jets, and at least one must have $E_T > 25$ GeV and $|\eta^{\text{det}}| \leq 2.5$. Jet energy is corrected for out-of-cone showering, calorimeter non uniformity, and the difference in calorimeter response between electrons and pions. Additional energy corrections are made to jets with soft muon tags to account for the muon and neutrino energies.

The missing transverse energy in the calorimeter ($\cancel{E}_T^{\text{cal}}$) is corrected for the presence of electrons, jets, and muons in the event. Events with additional isolated electrons or muons are rejected. We further require $\cancel{E}_T^{\text{JES}} > 15$ GeV and $15 < \cancel{E}_T < 200$ GeV, where $\cancel{E}_T^{\text{JES}}$ is the missing transverse energy with jet energy scale corrections applied and \cancel{E}_T also has corrections for the energy of an isolated muon. The upper bound of 200 GeV on \cancel{E}_T removes events with poorly reconstructed muon tracks.

Finally, misreconstructed events coming from multijet background where a jet fakes an electron or a muon are rejected by imposing cuts on the plane $\cancel{E}_T - \Delta\phi(l, \cancel{E}_T)$. These events tend to have the lepton aligned with the \cancel{E}_T and have low \cancel{E}_T .

V. ANALYSIS PROCEDURE

The analysis starts with a general set of preselection cuts designed to reject misreconstructed events and select a data sample that is modeled well by our background model. This is called the pretagged sample. After the preselection cuts we apply our b -tagging algorithms to separate signal events with heavy flavor from the W +light jet background. This forms our tagged sample. We use three different algorithms for b -jet tagging: (i) "Soft-Lepton Tagger" (SLT), which requires a muon associated with a jet. The muon is expected to come from the semileptonic decay of a B hadron or the cascade charm decay; (ii) "Secondary-Vertex Tagger" (SVT), a track-vertex reconstruction algorithm; and (iii) "Jet-Lifetime-Probability Tagger" (JLIP), a track impact-parameter based algorithm. The SVT and JLIP algorithms are *lifetime taggers* as they are sensitive to the decay length of the B hadron.

We ensure that we model the backgrounds properly at each level of selection cuts. For the W +jets background we model the shape of distributions by selecting orthogonal data samples that pass the preselection cuts but fail the b -tagging cut (and call it the untagged sample). For the misidentified lepton background we use data where the lepton isolation cut is reversed to simulate a lepton inside a jet faking isolation (called orthogonal sample). The $t\bar{t}$ and $Z \rightarrow \mu\mu$ + jets backgrounds are estimated using Monte Carlo.

An overview of the background estimation for the single top analysis is shown below in Fig. 3.

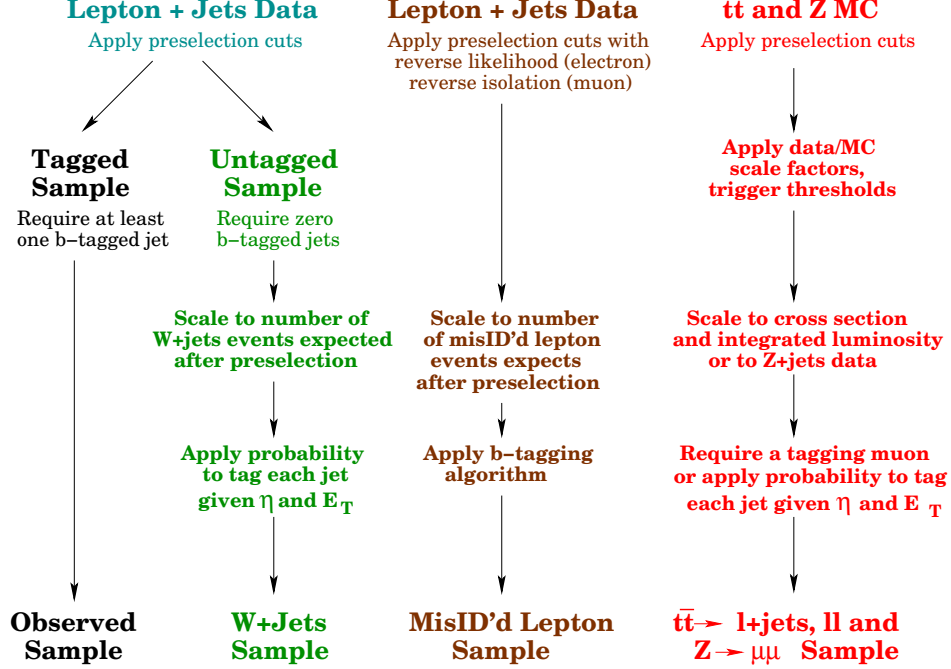


FIG. 3: Illustration of the starting samples and steps for each background measurement in the single top search.

A. Preselection and Final Cuts

There are two final selection requirements: there must be at least one b -tagged jet in the event; and the sum of the transverse energies of the lepton, two leading jets and missing energy ($H_T^{\nu jj}$) must be greater than 150 GeV.

Figure 4 shows that the $H_T^{\nu jj}$ cut is most effective at discriminating against the W +jets and fake-lepton backgrounds. No cuts are imposed specifically to reduce the $t\bar{t}$ background (such as an upper cut on the number of jets or on H_T), nor to further reject the fake-lepton background (such as a lower cut on M_T^W) as we found that they did not improve the expected cross section limits.

B. Signal Acceptances

Table I shows the results of the acceptances calculated for the s -channel, t -channel, and the combined $s+t$ -channel, after all event selections including b -tagging and the $H_T^{\nu jj} > 150$ GeV cut. Systematic errors, also shown, are described in Sec. VI. In the s -channel with SVT, a good tight isolated lepton is a 38% efficient. The b -tagging requirement is 50% efficient. The remaining cuts have an efficiency of 90% or better. The electron channel has similar efficiencies. The efficiencies are similar in the t -channel, except the b -tagging requirement is only 36% efficient due to the forward nature of one of the b -quarks. Both the electron decay and t -channel has similar efficiencies.

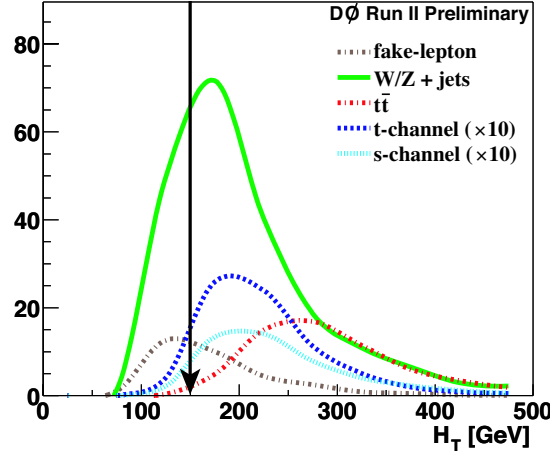


FIG. 4: Distributions of the sum of the transverse energies of the lepton, two leading jets, and missing transverse energy for the different signal and background sources after preselection cuts and b -tagging, for the combination of electron and muon channels, JLIP and SLT. The arrow shows where we apply cut, at 150 GeV.

	Percentage Acceptances of Single Top Signals		
	SLT	SVT	JLIP
<u>Electron Channel</u>			
tb	$0.475 \pm 0.011 \pm 0.063$	$1.209 \pm 0.015 \pm 0.200$	$1.218 \pm 0.015 \pm 0.167$
tqb	$0.295 \pm 0.009 \pm 0.043$	$0.897 \pm 0.011 \pm 0.164$	$0.907 \pm 0.011 \pm 0.150$
$tb+tqb$	$0.350 \pm 0.007 \pm 0.032$	$0.993 \pm 0.009 \pm 0.142$	$1.002 \pm 0.009 \pm 0.117$
<u>Muon Channel</u>			
tb	$0.437 \pm 0.011 \pm 0.057$	$0.962 \pm 0.013 \pm 0.183$	$0.961 \pm 0.013 \pm 0.167$
tqb	$0.264 \pm 0.008 \pm 0.042$	$0.674 \pm 0.009 \pm 0.146$	$0.712 \pm 0.010 \pm 0.142$
$tb+tqb$	$0.317 \pm 0.006 \pm 0.033$	$0.762 \pm 0.007 \pm 0.136$	$0.789 \pm 0.008 \pm 0.126$

TABLE I: Acceptances of the Monte Carlo signals for the final selection cuts. The values are given as a percentage of the *total cross section* for each process (including branching fraction). The first component of the error is from the MC statistics, and the second is the systematic contribution, which dominates (see Sec. VI for details).

C. Backgrounds in the Final Event Sample

We use the *Matrix Method* to find the normalizations for the misidentified-lepton and W +jets backgrounds in our preselected sample. For the shape we use the orthogonal sample, its size normalized to the result of the Matrix Method. The orthogonal sample has similar kinematic properties and flavor composition as the signal region.

The Matrix Method determines the W +jets (*real- l*) and misidentified-lepton background (*fake- l*) normalization using two datasets, one a subset of the other (a *loose* and *tight* sample). The first dataset, the *loose* sample, can be described as $N_{\text{loose}} = N^{\text{fake-}l} + N^{\text{real-}l}$. The second dataset represents the *tight* sample: $N_{\text{tight}} = \varepsilon_{\text{fake-}l} N^{\text{fake-}l} + \varepsilon_{\text{real-}l} N^{\text{real-}l}$. The ε represents the efficiency of a single cut that selects tight leptons. The ε is assumed to be different for real leptons and fake leptons. The choice cut is different, of course, for muons and electrons (isolation for the μ sample, and likelihood for the electron sample). The loose sample is our pretagged sample, but without the mentioned cut applied. We measure the real and fake efficiencies on independent samples, which allows us to solve for the number of real ($\varepsilon_{\text{real-}l} N^{\text{real-}l}$) and fake ($\varepsilon_{\text{fake-}l} N^{\text{fake-}l}$) leptons in our pretagged (tight) sample. We have called this method the *Matrix Method*.

The probability for an electron to pass the likelihood cut, found from a $Z \rightarrow ee$ data sample, is $\varepsilon_{\text{real-}e} = 0.891 \pm 0.006$. The fake-electron probability is found from a data sample for which is enriched with multijet events. $\varepsilon_{\text{fake-}e}$ varies as a function of electron E_T . Above 25 GeV it is 0.075, below it is $-0.012(E_T - 25) + 0.075$. The error, used as a systematic, is $\pm 50\%$. Though large, this systematic has minial effect on the final result (see Section VI).

The efficiency for a real muon to pass the isolation cut, determined in a $Z \rightarrow \mu\mu$ data sample, is $\varepsilon_{\text{real-}\mu} = 0.861 \pm 0.032$. The fake-muon probability is determined in a sample for which the missing transverse energy cut is reversed, $\cancel{E}_T < 15$ GeV, and is found to be: $\varepsilon_{\text{fake-}\mu} = 0.096 \pm 0.030$. No dependence was observed on the muon P_T .

To obtain the *tagged* W +jets yield, we estimate the probability for a jet in the pretagged W +jets sample to be

tagged. We start with the untagged sample scaled to the Matrix Method W +jets sample, and calculate a tagging probability for each event. This procedure not only gives an estimate for the yield but also reproduces the kinematic distributions of the W +jets background in the tagged signal sample.

The tag probability is calculated in the multijet data sample, with the the assumption that the flavor composition of jets in W +jets events is similar to the flavor composition of jets in the multijet sample. We have performed several cross checks to verify its validity, using Z +jets data samples and a W +2 jets data sample (requiring the sum of E_T of all objects in the event and the \cancel{E}_T to be: $H_T < 200$ GeV to reduce the $t\bar{t}$ content). We have found agreement in all of these comparisons within an uncertainty of 20%, which is used as a systematic error.

This tag probability, a flavor-inclusive tag-rate function (TRF), is determined from multijet data chosen to have similar kinematic properties to the signal data. For the SLT tagger, the TRF is parametrized as a function of jet E_T , η^{det} , and ϕ and derived from a large sample containing mostly ≥ 4 jets.

For the lifetime taggers we derive the flavor-inclusive TRFs on a sample with jet multiplicities more similar to those in this analysis (≥ 2 jets). The TRFs thus determined are also applied to the sample with higher jet multiplicities as a cross check. We found that the tag rate changes as a function of the number of jets in the event in this sample, and thus scale the lifetime flavor-inclusive TRFs accordingly: the tag-rate functions are scaled by 0.965 ± 0.048 for two-jet events and by 1.180 ± 0.059 for three-or-more jet events to account for differences in heavy flavor content expected in different event topologies. No such effect was observed for the SLT tagger.

After proper weighting and normalization of the W +jets and misidentified lepton samples the content in the final tagged sample is determined by applying the $H_T^{\nu jj}$ cut to obtain the yield (see Tab. III).

The $t\bar{t}$ and $Z \rightarrow \mu\mu$ background are determined from Monte Carlo; however, for $Z \rightarrow \mu\mu$ the number of events is normalized using the number of $Z \rightarrow \mu\mu + 2$ to 4 jets events observed in the data.

VI. SYSTEMATIC UNCERTAINTIES

Most background contributions are calculated directly from data, as described in Sec. V. We assign a systematic uncertainty of $\pm 20\%$ to the flavor-inclusive tag-rate functions. This is the largest contribution to the overall background uncertainty because it applies to the largest background source.

We also assign uncertainties to the factors used to scale the misidentified lepton and W +jets backgrounds. These uncertainties, however, are anti-correlated because the normalization factors are determined through the Matrix Method (see Sec. V C). Hence, these normalization uncertainties largely cancel when considering the combined misidentified lepton and W +jets background. The resulting overall uncertainty on this combined data background ranges from $\pm 16\%$ to $\pm 19\%$.

Table II lists the systematic errors taken into account for the yield estimates derived from Monte Carlo. All the systematics are individually calculated for each Monte Carlo sample which accounts for the range of some of the errors. These systematic errors are applied to the Monte Carlo samples, which account for a small part of the background in the single top search.

Monte Carlo Systematic Uncertainties	
$t\bar{t}$ theory and mass	$\pm 18\%$
$s(t)$ -channel theory	$\pm 15\% (\pm 16\%)$
Normalization of σ for $Z \rightarrow \mu\mu + \text{jets}$	$\pm 16\%$
Jet Energy Scale	$\pm 2 - \pm 13\%$
Trigger Modeling	$\pm 5 - \pm 13\%$
SVT and JLIP TRFs	$\pm 7 - \pm 12\%$
MC Jet Fragmentation	$\pm 5\% - \pm 7\%$
Integrated Luminosity	$\pm 6.5\%$
μ ID MC Scaling	$\pm 6.3\%$
Jet ID	$\pm 4\%$
$\text{BR}(B \rightarrow \mu X)$	$\pm 2.6\%$
e ID MC Scaling	$\pm 2.4\%$
Branching Fraction for $t\bar{t}$, s , t -channel	$\pm 2\%$
Jet Energy Resolution	$\pm 2\%$
SLT μ ID MC Scaling	$\pm 0.6\%$

TABLE II: Summary of the systematic errors on the Monte Carlo based event yields. Some of the systematic errors are relevant to only some of the decay channels. See text for further comments.

The resulting combined uncertainty for MC background yields is between $\pm 22\%$ and $\pm 27\%$ depending on the channel and source, except for the $Z \rightarrow \mu\mu + \text{jets}$ background which has an uncertainty of $\pm 34\%$ (due mostly to a large trigger systematic). The largest contribution to the MC yield uncertainties are due to the uncertainties on the cross sections used for normalization. The uncertainty on the signal acceptance varies between $\pm 14\%$ and $\pm 22\%$. The largest contributions to the acceptance uncertainty come from the trigger model and from the flavor-dependent tag-rate functions. The flavor-dependent tag-rate functions are calculated on data for jets from light quarks and heavy flavor quarks individually. A charm flavor-dependent TRF is derived from the b -quark TRF and scaled by the ration of charm to b -quark tagging in Monte Carlo.

VII. RESULTS

Table III shows the numbers of events for each of the signals, combinations of signals, and backgrounds. The $W + \text{jets}$ and multijet misidentified-lepton backgrounds are combined since the Matrix Method creates a strong anti-correlation in most of their uncertainties. The uncertainties have been combined taking into account these anti-correlations.

The shapes of several key distributions have been examined – the jet multiplicity in exclusive multiplicity bins, the transverse mass of the reconstructed W boson, and H_T^{lvjj} of the event. Figure 5 shows these distributions for both tag versions of the analysis. Each plot shows the combination of the electron and muon channel. Each row corresponds to a different combination of taggers: the top row to the combination of JLIP and SLT, while the bottom row corresponds to the combination of SVT and SLT. Section X has a similar plot showing the individual contributions of the background sources (but not the systematic errors).

	Expected Signal and Background Event Yields in Run II Data					
	Electron Channel			Muon Channel		
	SLT	SVT	JLIP	SLT	SVT	JLIP
Signals						
MC $t\bar{b}$	0.65 ± 0.14	1.79 ± 0.43	1.81 ± 0.40	0.61 ± 0.12	1.34 ± 0.34	1.34 ± 0.33
MC tqb	0.91 ± 0.20	3.00 ± 0.73	3.03 ± 0.71	0.83 ± 0.21	2.11 ± 0.57	2.23 ± 0.58
MC $t\bar{b} + tqb$	1.57 ± 0.30	4.79 ± 1.05	4.84 ± 0.99	1.44 ± 0.28	3.45 ± 0.85	3.57 ± 0.83
Backgrounds						
MC $t\bar{t} \rightarrow l + \text{jets}$	7.05 ± 1.66	18.93 ± 4.51	19.26 ± 4.71	6.09 ± 1.50	14.71 ± 3.55	14.83 ± 3.80
MC $t\bar{t} \rightarrow ll$	2.67 ± 0.60	5.18 ± 1.25	5.22 ± 1.24	1.96 ± 0.43	4.34 ± 1.10	4.36 ± 1.11
MC $Z \rightarrow \mu\mu + \text{jets}$	—	—	—	10.29 ± 3.48	—	—
$W + \text{jets}$ yield	20.2 ± 4.7	41.9 ± 9.2	58.8 ± 12.9	19.0 ± 3.9	41.4 ± 8.9	53.8 ± 11.6
Fake- l yield	5.5 ± 3.1	3.9 ± 2.2	3.4 ± 1.9	4.9 ± 1.7	13.3 ± 4.7	14.0 ± 5.0
$W + \text{jets} + \text{fake-}l$ sum	25.7 ± 4.1	45.8 ± 8.9	62.2 ± 12.5	22.4 ± 3.9	48.41 ± 8.8	60.0 ± 11.4
Sum of bkgds for $t\bar{b}$	36.3 ± 4.8	72.9 ± 10.8	89.7 ± 14.0	41.6 ± 6.2	69.6 ± 10.1	81.5 ± 12.5
Sum of bkgds for tqb	36.1 ± 4.7	71.7 ± 10.7	88.5 ± 13.9	41.4 ± 6.1	68.8 ± 10.0	80.6 ± 12.5
Sum of bkgds for $t\bar{b} + tqb$	35.4 ± 4.7	69.9 ± 10.5	86.7 ± 13.8	40.8 ± 6.1	67.5 ± 10.0	79.2 ± 12.4
Observed events	54	63	78	43	75	70

TABLE III: Summary of the yields of signal and background events in the electron and muon channels after final selection, with combined errors. The summed background for an individual single top production mode includes the other single top mode as part of that background.

We use the numbers of observed events to calculate upper bounds on the single top production cross sections using a Bayesian method, cross checked with a modified frequentist method. When determining the upper bound on the s -channel (t -channel) cross section, single top production from the t -channel (s -channel) is included as part of the background. The total number of events in each analysis channel is the test statistic used to discriminate between the signal-plus-background hypothesis and the background-only hypothesis. Uncertainties are taken into account in the limit calculations by performing a large number of Monte Carlo experiments. For each experiment, a new set of “smeared” signal and background rates is obtained and from these distributions, the numbers of signal and background events for this particular Monte Carlo experiment are generated. Correlations between systematic uncertainties and between different analysis channels and background sources are fully taken into account. Results are very similar (as expected) between the two calculation methods.

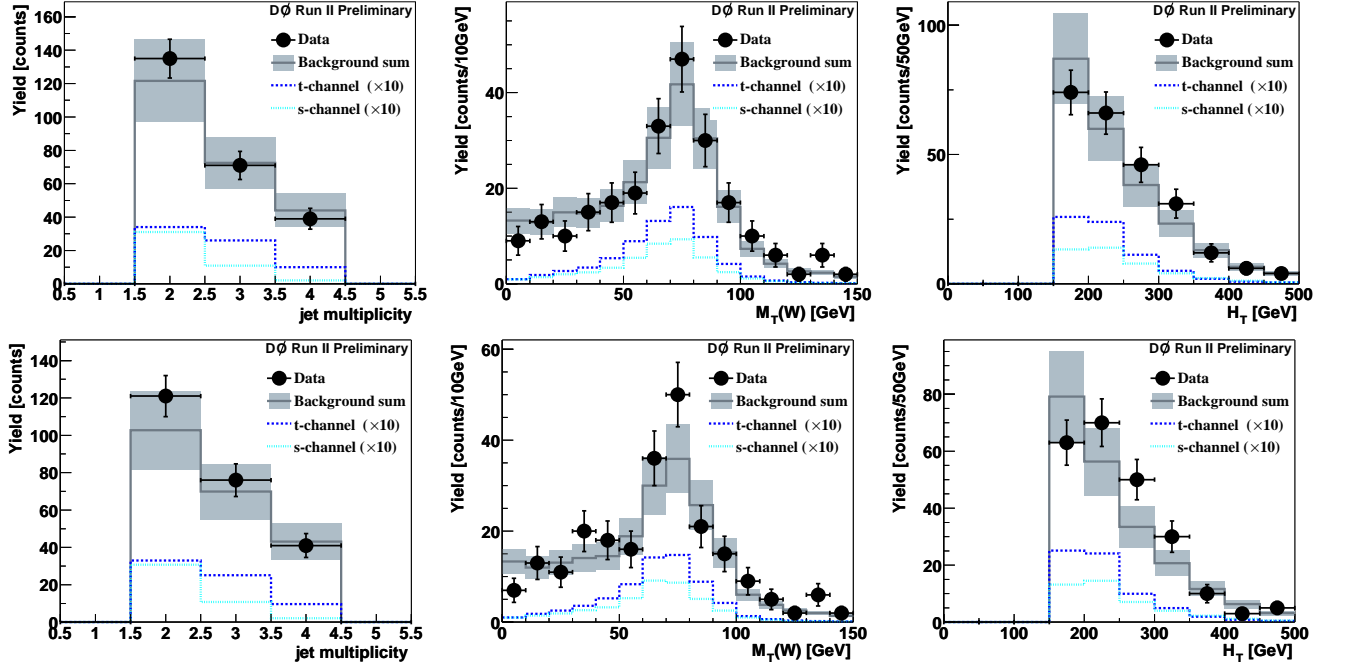


FIG. 5: Distributions of the number of good jets, the transverse mass of the W boson, and the scalar sum of the transverse energy of the electron, neutrino, and two highest- E_T jets, for the electron and muon channel combined. The upper row shows the plots for the combination of JLIP and SLT, the lower row for the combination of SVT and SLT. The sum of the $t\bar{t}$, W +jets, and fake- l background contributions is shown as the gray line with shaded error band. The two signal contributions $t\bar{b}$ and tqb are multiplied by 10 in the plots.

The expected and measured 95% confidence level upper limits on the production cross section of single top events are summarized in Tab. IV for the Bayesian method. Our final results are for the electron and muon channels combined with both the SLT and SVT tagging methods (the SVT tagger has slightly better expected cross section limit than the JLIP tagger).

95% CL Expected / Measured Upper Limits on the Single Top Production Cross Sections After Final Selection, with Systematics, Bayesian				
Channel	Electron	Muon	$e + \mu$	$e + \mu$ with SLT
<u>s-channel</u>				
SLT	26 / 53	33 / 35	22 / 40	
SVT	18 / 14	24 / 27	17 / 14	16 / 19
JLIP	20 / 16	26 / 21	20 / 15	17 / 22
<u>t-channel</u>				
SLT	42 / 81	56 / 59	37 / 67	
SVT	24 / 20	35 / 41	24 / 20	23 / 25
JLIP	27 / 22	37 / 29	27 / 21	25 / 30
<u>s- and t-channel</u>				
SLT	35 / 72	45 / 49	30 / 57	
SVT	21 / 18	29 / 36	20 / 18	20 / 23
JLIP	24 / 20	32 / 26	23 / 19	22 / 30

TABLE IV: The expected and measured 95% confidence level expected upper limits on the production cross section (in pb) of single top events, taking into account systematic uncertainties, after the final selection cuts are applied, using the Bayesian method.

Figure 6 shows the corresponding Bayesian posterior probability densities for the SVT/SLT taggers for the combination of electron plus muon channel. The JLIP/SLT posterior probability densities are similar. The excess of data events observed in the electron/SLT channel is evident in the plots, the SLT posterior density peaks at a non-zero

cross section. We believe the current excess to be due to a statistical fluctuation. This is supported from an ongoing analysis in the same channel using new additional data which, if included, does not show an excess. The SVT and JLIP channels by contrast do not observe any excess. Since these have higher acceptance, they dominate in the combination with SLT. Hence the SVT/SLT combination limit is only slightly worse than the SVT limit by itself.

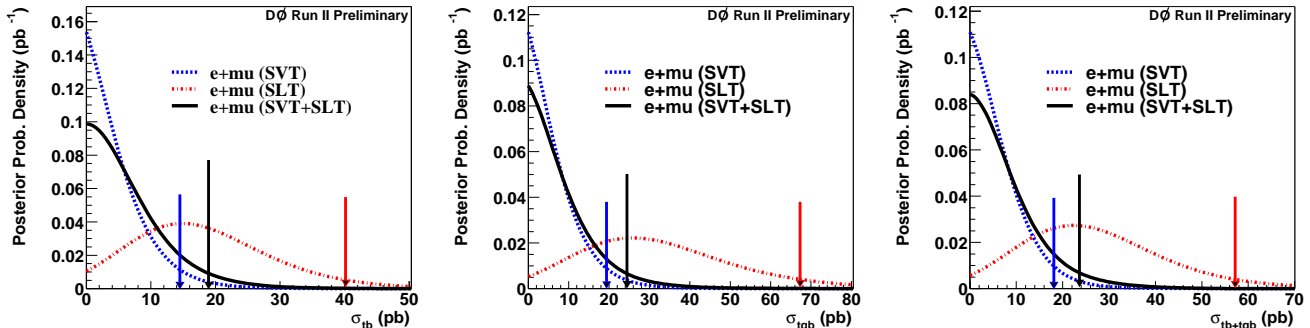


FIG. 6: Distributions of the Bayesian posterior probability density for the combination of electron and muon channels for the three different signal channels: s -channel (tb , left), t -channel (tqb , middle), and the combination of s - and t -channels (right).

VIII. SUMMARY

We have performed a search for electroweak production of top quarks in the electron+jets and muon+jets decay channels. The measurements use ~ 156 to 169 pb^{-1} of data from Run II of the Fermilab Tevatron collider collected at a center of mass energy of 1.96 TeV. The data were collected with the DØ detector between August 2002 and September 2003. We see no excess events in the data so we set an upper limit at 95% confidence level on the cross section of 19 pb for the s -channel process, 25 pb for the t -channel process, and 23 pb for the combined s and t channel process.

IX. ACKNOWLEDGMENTS

We thank the staffs at Fermilab and collaborating institutions, and acknowledge support from the Department of Energy and National Science Foundation (USA), Commissariat à l’Energie Atomique and CNRS/Institut National de Physique Nucléaire et de Physique des Particules (France), Ministry of Education and Science, Agency for Atomic Energy and RF President Grants Program (Russia), CAPES, CNPq, FAPERJ, FAPESP and FUNDUNESP (Brazil), Departments of Atomic Energy and Science and Technology (India), Colciencias (Colombia), CONACyT (Mexico), KRF (Korea), CONICET and UBACyT (Argentina), The Foundation for Fundamental Research on Matter (The Netherlands), PPARC (United Kingdom), Ministry of Education (Czech Republic), Natural Sciences and Engineering Research Council and WestGrid Project (Canada), BMBF (Germany), A.P. Sloan Foundation, Civilian Research and Development Foundation, Research Corporation, Texas Advanced Research Program, and the Alexander von Humboldt Foundation.

X. APPENDIX: PLOTS

Figure 7 shows the contributions of each background (and the single top signal) to distributions of the jet multiplicity in exclusive multiplicity bins, the transverse mass of the reconstructed W boson, and $H_T^{\ell\nu jj}$ after all selection cuts. Each plot shows the combination of the electron and muon channel. Each row corresponds to a different combination of taggers: the top row to the combination of JLIP and SLT, while the bottom row corresponds to the combination of SVT and SLT. No systematic errors are shown.

[1] F. Abe *et al.*, (CDF Collaboration), “Observation of Top Quark Production in $p\bar{p}$ Collisions.” *Phys. Rev. Lett.* **74**, 2626 (1995).

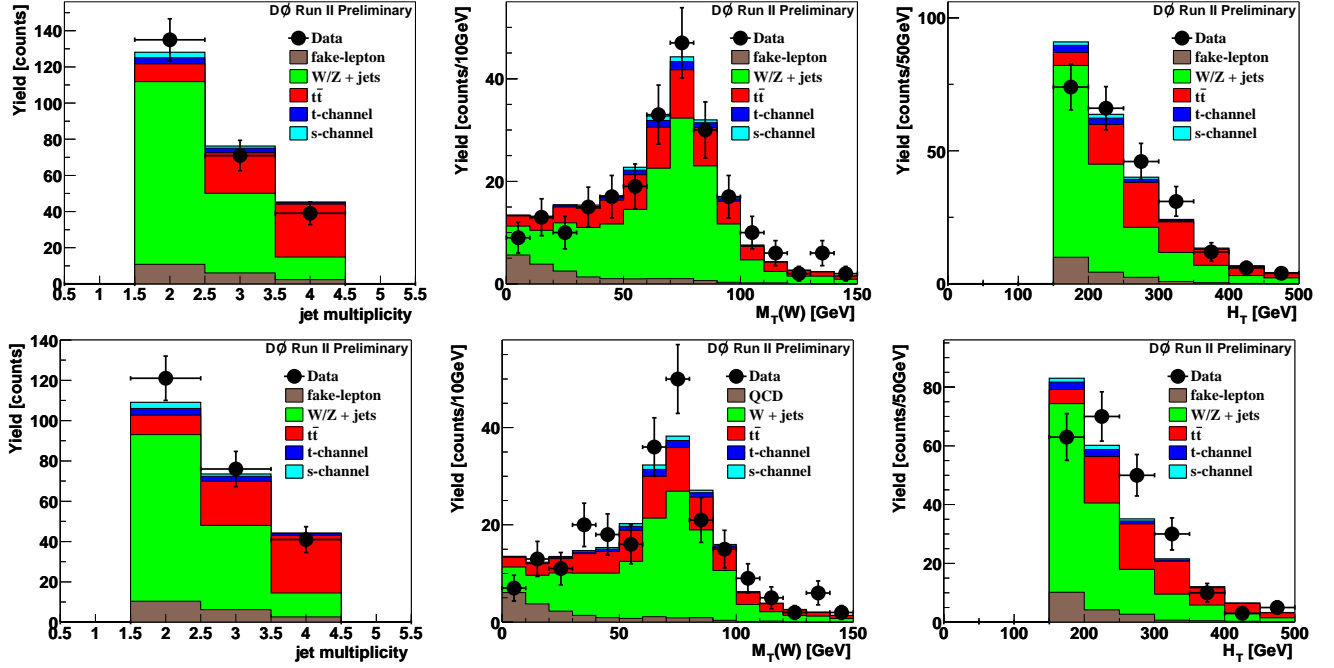


FIG. 7: Distributions of the number of good jets, the transverse mass of the W boson, and the scalar sum of the transverse energy of the electron, neutrino, and two highest- E_T jets, for the electron and muon channel combined for the different background sources. The upper row shows the plots for the combination of J1IP and SLT, the lower row for the combination of SVT and SLT.

- [2] S. Abachi *et al.*, (DØ Collaboration), “Observation of the Top Quark,” *Phys. Rev. Lett.* **74**, 2632 (1995).
- [3] The CDF Collaboration, The DØ Collaboration, and the Tevatron Electro-Weak Working Group, “Combination of CDF and DØ Results on the Top-Quark Mass,” DØ Note 4417, hep-ex/0404010 (April 2004).
- [4] The LEP Collaborations, the LEP Electroweak Working Group, the SLD Electroweak and Heavy Flavor Groups, “A Combination of Preliminary Electroweak Measurements and Constraints on the Standard Model,” hep-ex/0312023, (December 2003).
- [5] M. Beneke *et al.*, “Top Quark Physics,” in *Standard Model Physics (and more) at the LHC*, hep-ph/0003033, (March 2000).
- [6] D. Chakraborty, J. Konigsberg, and D. Rainwater, “Review of Top Quark Physics,” to appear in *Ann.Rev.Nucl.Part.Sci.*, hep-ph/0303092, (March 2003).
- [7] A.P. Heinson, A.S. Belyaev and E.E. Boos, “Single Top Quarks at the Fermilab Tevatron,” *Phys. Rev. D* **56**, 3114 (1997).
- [8] T. Stelzer, Z. Sullivan and S. Willenbrock, “Single-Top-Quark Production via W -Gluon Fusion at Next-to-Leading Order,” *Phys. Rev. D* **56**, 5919 (1997).
- [9] B.W. Harris, E. Laenen, L. Phaf, Z. Sullivan and S. Weinzierl, “The Fully Differential Single Top Quark Cross Section in Next-to-Leading Order QCD,” *Phys. Rev. D* **66**, 054024 (2002).
- [10] M.C. Smith and S. Willenbrock, “QCD and Yukawa Corrections to Single-Top-Quark Production via $q\bar{q} \rightarrow t\bar{b}$,” *Phys. Rev. D* **54**, 6696 (1996).
- [11] B. Abbott *et al.*, (DØ Collaboration), “Search for Electroweak Production of Single Top Quarks in $p\bar{p}$ Collisions,” *Phys. Rev. D* **63**, 031101 (2001).
- [12] V.M. Abazov *et al.*, (DØ Collaboration), “Search for Single Top Quark Production at DØ Using Neural Networks,” *Phys. Lett. B* **517**, 282 (2001).
- [13] D. Acosta *et al.*, (CDF Collaboration), “Search for Single Top Quark Production in $p\bar{p}$ Collisions at $\sqrt{s} = 1.8$ TeV,” *Phys. Rev. D* **65**, 091102 (2002).
- [14] D. Acosta *et al.*, (CDF Collaboration), “Optimized Search for Single Top Quark Production at the Fermilab Tevatron,” *Phys. Rev. D* **69**, 052003 (2004).
- [15] B. Abbott *et al.*, (DØ Collaboration), “The Upgraded DØ Detector,” in preparation, to be submitted to *Nucl. Instrum. Meth.*; S. Abachi *et al.*, (DØ Collaboration), “The DØ Detector,” *Nucl. Instrum. Meth. A* **338**, 185 (1994).
- [16] A. Pukhov *et al.*, Report INP-MSU 98-41/542, hep-ph/9908288; <http://theory.sinp.msu.ru/comphep>.
- [17] E. Boos, L. Dudko, V. Savrin and A. Sherstnev, in preparation; E. Boos, L. Dudko and V. Savrin, CMS Note 2000/065.
- [18] T. Sjostrand *et al.*, “PYTHIA 6.3, Physics and Manual,” LU-TP-03-38, hep-ph/0308153 (2003).
- [19] S. Jadach, Z. Was, R. Decker and J. H. Kuhn, “The tau decay library TAUOLA: Version 2.4,” *Comput. Phys. Commun.* **76**, 361 (1993).
- [20] N. Kidonakis and R. Vogt, “Next-to-Next-to-Leading Order Soft-Gluon Corrections in Top Quark Hadroproduction,” *Phys. Rev. D* **68**, 114014 (2003).

- [21] D. J. Lange, “The Evtgen Particle Decay Simulation Package,” Nucl. Instrum. Meth. A **462**, 152 (2001).
- [22] M.L. Mangano, M. Moretti, F. Piccinini, R. Pittau, and A.D. Polosa, “ALPGEN, a Generator for Hard Multiparton Processes in Hadronic Collisions,” J. High Energy Physics **0307**, 001 (2003).
- [23] J. Pumplin *et al.* (CTEQ collaboration), “New Generation of Parton Distributions with Uncertainties from Global QCD Analysis,” hep-ph/0201195 (2002).
- [24] R. Brun *et al.*, CERN Program Library Writeup W5013 (1993).